Nonsinusoidal buckling of thin gold films on elastomeric substrates

Huiyang Fei and Hanqing Jiang[a)]
Department of Mechanical and Aerospace Engineering, Arizona State University, Tempe, Arizona 85287

Dahl-Young Khang[b)]
Department of Materials Science and Engineering, Yonsei University, Seoul 120-749, Korea

(Received 17 December 2008; accepted 2 February 2009; published 24 March 2009)

Buckling of stiff thin films on compliant substrates represents a variety of applications, ranging from stretchable electronics to micro-nanometrology. Different but complementary to previously reported sinusoidal buckling waves, this letter presents a nonsinusoidal surface profile of buckled thin Au films on compliant substrates, specifically, a secondary dip on top of buckling wave or rather broadened wave top with very sharp trough. This nonsinusoidal profile is likely due to tension/compression asymmetry, i.e., different strengths in tension and compression resulted from the polycrystalline, grained microstructure of metal film. Finite element analysis with asymmetric tension/compression material model has reproduced the experiments well qualitatively. © *2009 American Vacuum Society.* [DOI: 10.1116/1.3089244]

I. INTRODUCTION

Nonlinear buckling of thin, high modulus plates/thin films on compliant substrates represents a classical problem in mechanics and physics. Over the past several decades, numerous theoretical and experimental studies of this phenomenon have been performed.[1,2] Although buckling has historically been viewed as a mechanism for structural failure, Whitesides' pioneering work[3] in the late 1990s showed that this behavior can be controlled in micro- and nanoscale systems to generate interesting structures with well defined geometries and dimensions in the 100 nm–100 μm range. These observations created renewed interest in this area which persists today, with many active research groups currently exploring basic scientific aspects[4] as well as applications in stretchable electronics,[5–9] micro- and nanoelectromechanical systems,[10] tunable diffraction and phase grating,[11,12] force spectroscopy in cells,[13] biocompatible topographic matrices for cell alignment,[14,15] high precision micro- and nanometrology methods,[16–19] and pattern formation for micro-/nanofabrication.[3,20–24] In these systems, buckling is realized in thin films deposited, typically by vapor phase or physical transfer processes, onto prestrained elastomeric substrates. Releasing the prestrain can create "wavy" structures. The designs of these systems can range from simple layouts consisting of uniform films on flat substrates to complex lithographically patterned films on substrates with structures of relief embossed on their surfaces. The diversity of wavy geometries enabled by these strategies creates considerable engineering flexibility in the types of structures that can be formed.

Yet, all the previous works on mechanical buckling, both experimental work and theoretical analysis, have either observed or assumed only an ideally sinusoidal profile of buckled surface. Intuitively, ideally sinusoidal buckling wave is only one of the possible buckling modes, and other modes may also exist. In this letter, we present a nonsinusoidally buckled surface profile for the first time. The buckled surface profile was found to depend on film thickness, prestrain, and the release rate of prestrain. This nonsinusoidal profile is likely due to asymmetry of the elastic behaviors of film material in tension and compression, which originates from the polycrystalline microstructural nature of material. More specifically, the thin film material with grain size comparable to the thin film thickness deforms easier in tension than in compression. Using a hypothetical elasticity model that reflects this asymmetric elastic behavior under tension and compression, finite element analysis yielded nonsinusoidal surface profile, qualitatively similar to our experimental observations.

II. EXPERIMENT

The Au film was deposited on elastomeric substrate, polydimethylsiloxane (PDMS), by electron-beam evaporation, with Ti (3 nm) as an adhesion layer. For a patterned metal film deposition, a shadow mask made from thin (25 μm) polyimide (PI) film was used. The PI shadow mask was fabricated by laser micromachining, and had various pattern features such as line, triangle, rectangle, circle, etc. For an elastomeric substrate, Sylgard 184 (Dow, USA) was formulated at 10:1 ratio (by weight) of base resin to curing agent and cured at 70 °C for >4 h. The cured PDMS (3–5 mm thick) was cut into rectangular slab of $\sim 2 \times 4$ cm^2. To apply prestrain on the PDMS substrate during metal deposition, the PDMS slab was held and stretched to a predefined length on

a)Electronic mail: hanqing.jiang@asu.edu
b)Electronic mail: dykhang@yonsei.ac.kr

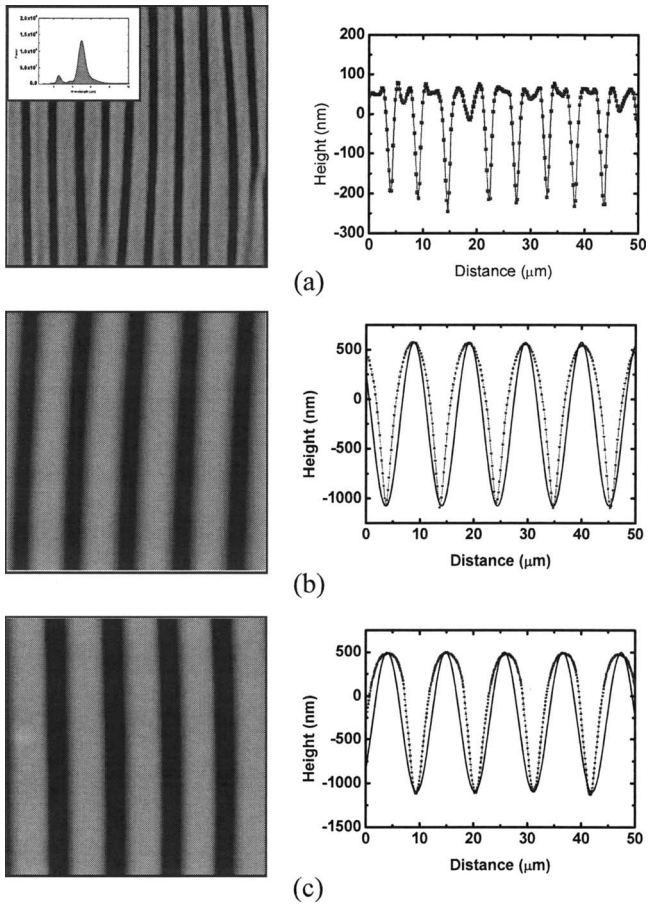

FIG. 1. Effect of Au film thickness on the buckling profile. (a) 50 nm, (b) 100 nm, and (c) 150 nm. Left column shows the plane-view AFM images and the right column denotes the line-cut surface profile of corresponding images [blue lines in (b) and (c) are from the sinusoidal function fit]. The inset in (a) is the power spectrum of AFM image.

a homemade stretching stage. The prestrain was measured from the ratio of the length change of PDMS as $\varepsilon_{pre}=(L-L_0)/L_0$, where L_0 and L are the initial and stretched lengths of PDMS substrate, respectively.

The soft nature of PDMS substrate enabled conformal contact of PI shadow mask on it. After the Au evaporation, the PDMS surface looked cloudy and hazy under the room light when released from the stretching stage due to diffusive light scattering from the buckled Au surface. For the characterization of buckled surface, optical and atomic force microscopies were used. Especially, line-cut surface profile from the atomic force microscopy (AFM) measurement yielded buckled morphology in great detail.

III. RESULTS AND DISCUSSION

Figure 1 shows the effect of Au film thickness on the buckling profile, where the prestrain was fixed at 20%. For a 50 nm thick Au film, shown in Fig. 1(a), the line-cut profile of the surface clearly shows the nonsinusoidal surface. The buckled surface is not an ideally sinusoidal wave shape. Rather, there are dips on top of each wave peak, and the troughs are very steep and sharp. Further, those dips on each wave peak are approximately located at the center, which is also confirmed from dual peaks on the power spectrum of buckled surface [inset of Fig. 1(a)]. In other words, an M-shaped buckling wave appears for a 50 nm thick buckled Au film. As the Au film thickness increases, dips on top of wave peaks disappear, as shown in Figs. 1(b) and 1(c). It is also noticed, however, that the profiles still do not fit to ideally sinusoidal waves (marked by blue solid line). Both the wave top and trough become slightly rounded and broadened as film thickness increases, although the wave troughs are still much steeper compared to wave peaks.

Another key factor in determining the shape of buckled surface profile is the level of prestrain. At the fixed Au film thickness of 100 nm, the prestrain was varied from 5% to

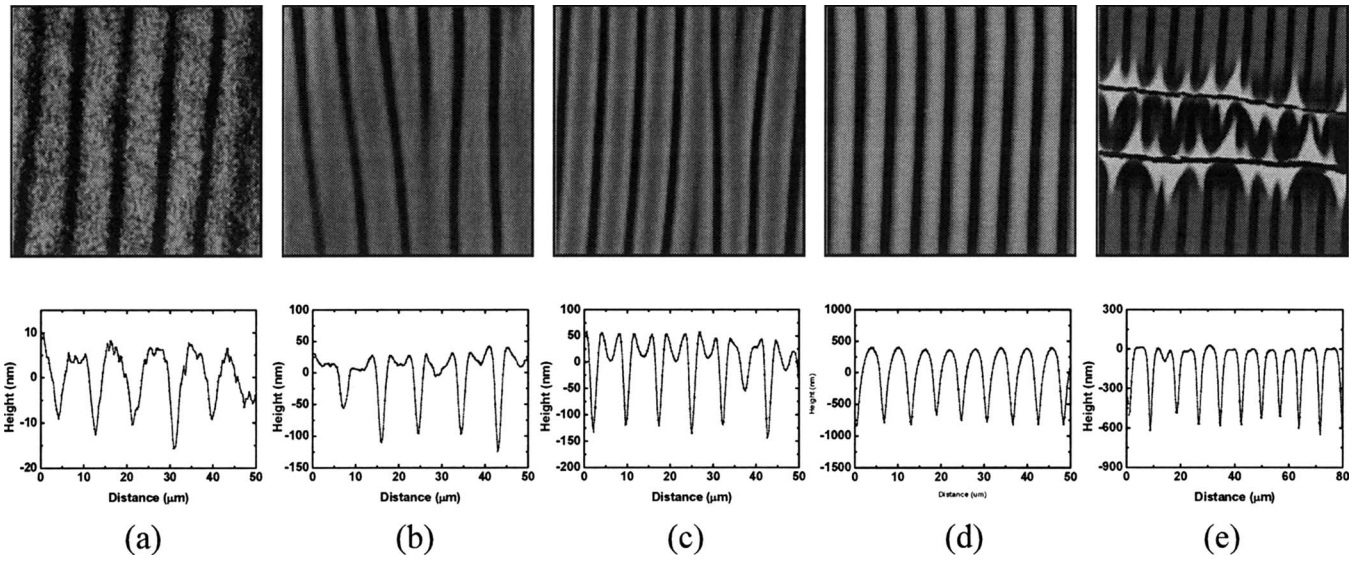

FIG. 2. Effect of prestrain on the buckling profile, for 100 nm thick Au film on PDMS. The prestrains were 5%, 10%, 20%, 30%, and 40%, from left to right, respectively. Top panel shows AFM images, and the corresponding line-cut profiles are shown in the bottom panel.

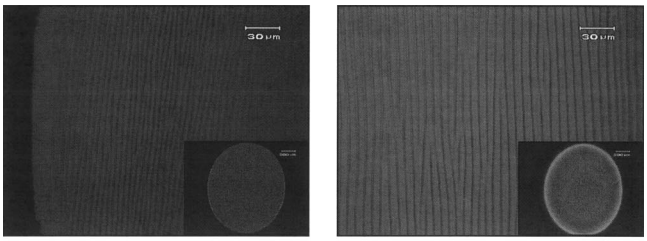

(a) (b)

FIG. 3. Effect of strain release rate on the buckling of 100 nm thick Au film on PDMS. The prestrain was 20% for both cases, but the prestrain was released (a) instantaneously, or (b) slowly. The insets show lower magnification images by optical microscope.

40%, and corresponding AFM images and line-cut profiles were obtained and are shown in Fig. 2. One common feature in Fig. 2 is that the wave troughs are much steeper and sharper than wave peaks, regardless of prestrain level. On the other hand, the shape of wave peaks depends on the prestrain value. At the lowest prestrain investigated here (5%), the wave peak seemed to have rough, corrugated surface, as shown in Fig. 2(a). However, as the prestrain increased to 10% and 20%, dips on top of each wave peaks started to appear, as shown in Figs. 2(b) and 2(c), respectively. Upon further increase in prestrain to 30%, the wave top became rounded and the dips on each wave peak disappeared, as shown in Fig. 2(d). Finally, the film was cracked along the compression direction when the prestrain was too high, namely 40%, as shown in Fig. 2(e). The profile, which shows rather flattened wave peaks with very steep valleys, is measured at far from the cracks. Upon closer observation, there are reminiscent of dips on wave peaks around cracked region. Cracks release the strain locally, which leads to different strain states around and far from the cracks.

Note here that the buckled surface showed quite different profiles under the same prestrain, namely, Au (100 nm) film with 20% prestrain cases, shown in Figs. 1(b) and 2(c). This is due to the difference in strain release rate. The prestrain was released almost instantaneously for the experiment shown in Fig. 1(b), or very slowly (over ~5 min) for that in Fig. 2(c). To obtain a larger view of these samples, the optical microscopy images of those samples are shown in Fig. 3. For the fast release of prestrain, it seems that the sample surface has lots of particles [inset of Fig. 3(a)]. Upon magnification, it is realized that these are not particles but discontinuities or structural defects of buckling waves, as shown in Fig. 3(a). When the release rate is very low, those defects are greatly reduced and thus the surface appeared brighter than the surface having many defects [Fig. 3(b)]. The reduction in defects can clearly be seen in the magnified image shown in Fig. 3(b), where the buckling waves are well aligned with few defects. Also, there is nonbuckled area along the circular edge, which looks bright yellow due to specular reflection of light from the flat Au film, as shown in the inset of Fig. 3(b). Similar results, i.e., the dependence of structural defect density on the strain release rate, were previously reported,[12] although the exact mechanism is yet to be found. The results in this work revealed that the difference in strain release rate may lead to very different buckling profiles, let alone the difference in structural perfection. Further works are needed to clarify the effect of strain release rate on the buckling profile, both experimentally and theoretically.[21–24]

IV. FINITE ELEMENT MODELING

Finite element analysis of this Au/PDMS buckling system was performed. The hypothesis of the buckling behavior featured with nonsinusoidal profile is tension/compression asymmetry. When the thickness of gold thin film decreases to nanoscale that is comparable to the grain size, it is expected that the Au thin film exhibit asymmetries in tension and compression, which has been observed[25,26] for Au thin films with nanoscale thickness. To qualitatively understand the influence of the tension/compression asymmetry on the buckling behavior, the film material was modeled mathematically as [Fig. 4(a)]

$$\sigma(\mathrm{MPa}) = \begin{cases} -90(-\varepsilon/0.009)^{0.3}, & \varepsilon < -0.9\% \\ 10^4\varepsilon, & -0.9\% \leqslant \varepsilon \leqslant 0.3\% \\ 30(\varepsilon/0.003)^{0.1}, & \varepsilon > 0.3\%. \end{cases} \quad (1)$$

The soft substrate is modeled by a linear elastic material with Young's modulus of 2 MPa and Poisson's ratio of 0.49. In

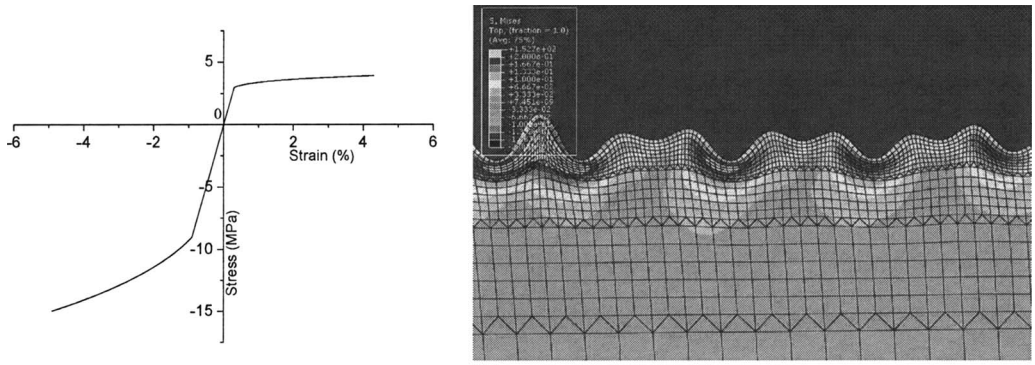

(a) (b)

FIG. 4. (a) Hypothetical elastic model for tension/compression asymmetry. (b) Buckled surface profile from finite element analysis using model shown in (a).

other words, the initial elastic modulus of thin film is the same (10 GPa) for tension/compression; however, the yield strain for compression (−0.9%) is larger than that for tension (0.3%). After yielding, the tensile modulus is set to be smaller than the compressive modulus.

The finite element analysis consists of a 3 mm thick PDMS substrate and a 100 nm thick Au thin film. The length of the two-dimensional system is 1 mm. The thin film is modeled by the beam elements (B21 in the ABAQUS finite element program). The substrate is modeled by the four-node plane-strain element (CPE4). The stress-free thin film is attached to the prestretched substrate by sharing the same nodes at the thin film/substrate interface. To ensure the beam element (B21) is compatible with the two-dimensional plane-strain solid elements (CPE4) in the substrate, the rotational degree of freedom in the beam elements is constrained. To overcome the difficulties of this analysis, namely, extremely large (up to 10^5) elastic mismatch between thin film and substrate, and extremely large (up to 10^4) difference in the film and substrate thickness, very fine mesh (with the smallest element size of $0.4\times0.4\ \mu m^2$) near the film/substrate interface and very small step increment (less than 10^{-2}) are used to ensure the convergent results. The finite element analysis starts from determining the eigenvalues and eigenmodes of the stress-free thin film/prestretched substrate system. The first sinusoidal eigenmode is used as initial small geometrical imperfection to trigger the buckling of the system. The imperfections are always small enough to ensure that the solution is accurate. Then the prestrain in PDMS substrate is released to model the experiment.

The finite element analysis found that the sinusoidal imperfections lead to nonsinusoidal buckling profile if the thin film materials have asymmetries in tension and compression. Figure 4(b) shows nonsinusoidal waves featured with dips on top of wave peaks for 2.1% prestrain. The analysis also found that the strain energy of the buckled thin film with nonsinusoidal wave is even lower than that with sinusoidal wave for almost the same prestrain (2.07%), which suggests that the nonsinusoidal wave is more energetically favorable for such thin film with asymmetric tension/compression behavior. Due to numerical singularity at the peak or valley of the buckling wave, it is difficult to reproduce the sharp trough in the finite element analysis.

Such finite element analysis verifies our hypothesis that the non-sinusoidal buckling wave results from the asymmetric tension/compression behavior of the thin film. With the increase of the thickness of thin film, this tension/compression asymmetry is gradually invisible and the thin film behaviors more like an isotropic elastic materials. Thus the sinusoidal buckling wave is dominant as shown in our experiments. A quantitative analytical model will be developed to understand this process later on.

V. CONCLUSION

In summary, nonsinusoidal buckling profile of buckled Au film on PDMS was demonstrated experimentally in this work. The detailed shapes of the surface profiles were all found to deviate from the ideal sinusoidal shape and to depend on the film thickness, the level of prestrain, and the strain release rate. This nonsinusoidal profile is likely due to asymmetric behavior of film material in tension and compression. To check this hypothesis, finite element analysis was performed using asymmetric material behavior in tension and compression. The calculation results indeed reproduced the experimental data reasonably well, at least qualitatively. Future works will include the development of analytic model for this nonideal behavior, and the effect of this nonsinusoidal buckling profile on the stretchability, electrical conductivity, etc.

ACKNOWLEDGMENTS

H. Jiang acknowledges the support from the National Science Foundation under Grant No. DMI-0328162. D.-Y. Khang acknowledges financial support from the Yonsei University Research Fund of 2008, and "System IC 2010" project of Korea Ministry of Commerce, Industry and Economy.

[1] H. G. Allen, *Analysis and Design of Structural Sandwich Panels* (Pergamon, New York, 1969).
[2] S. P. Timoshenko and J. M. Gere, *Theory of Elastic Stability* (McGraw-Hill, New York, 1961).
[3] N. Bowden, S. Brittain, A. G. Evans, J. W. Hutchinson, and G. M. Whitesides, Nature (London) **393**, 146 (1998).
[4] H. Jiang, D.-Y. Khang, J. Song, Y. Huang, and J. A. Rogers, Proc. Natl. Acad. Sci. U.S.A. **104**, 15607 (2007).
[5] D.-Y. Khang, H. Jiang, Y. Huang, and J. A. Rogers, Science **311**, 208 (2006).
[6] D.-H. Kim *et al.*, Science **320**, 507 (2008).
[7] H. C. Ko *et al.*, Nature (London) **454**, 748 (2008).
[8] S. Wagner, S. P. Lacour, J. Jones, P. I. Hsu, J. C. Sturm, T. Li, and Z. Suo, Physica E (Amsterdam) **25**, 326 (2004).
[9] S. P. Lacour, S. Wagner, R. J. Narayan, T. Li, and Z. Suo, J. Appl. Phys. **100**, 014913 (2006).
[10] Y. Q. Fu *et al.*, Appl. Phys. Lett. **89**, 3 (2006).
[11] C. Harrison, C. M. Stafford, W. Zhang, and A. Karim, Appl. Phys. Lett. **85**, 4016 (2004).
[12] K. Efimenko, M. Rackaitis, E. Manias, A. Vaziri, L. Mahadevan, and J. Genzer, Nature Mater. **4**, 293 (2005).
[13] A. K. Harris, P. Wild, and D. Stopak, Science **208**, 177 (1980).
[14] X. Y. Jiang *et al.*, Langmuir **18**, 3273 (2002).
[15] A. I. Teixeira, G. A. Abrams, P. J. Bertics, C. J. Murphy, and P. F. Nealey, J. Cell. Sci. **116**, 1881 (2003).
[16] C. M. Stafford, S. Guo, C. Harrison, and M. Y. M. Chiang, Rev. Sci. Instrum. **76**, 5 (2005).
[17] C. M. Stafford *et al.*, Nature Mater. **3**, 545 (2004).
[18] C. M. Stafford, B. D. Vogt, C. Harrison, and R. Huang, Macromolecules **39**, 5095 (2006).
[19] E. A. Wilder, S. Guo, S. Lin-Gibson, M. J. Fasolka, and C. M. Stafford, Macromolecules **39**, 4138 (2006).
[20] N. Bowden, W. T. S. Huck, K. E. Paul, and G. M. Whitesides, Appl. Phys. Lett. **75**, 2557 (1999).
[21] W. T. S. Huck, N. Bowden, P. Onck, T. Pardoen, J. W. Hutchinson, and G. M. Whitesides, Langmuir **16**, 3497 (2000).
[22] J. S. Sharp and R. A. L. Jones, Adv. Mater. (Weinheim, Ger.) **14**, 799 (2002).
[23] P. J. Yoo, K. Y. Suh, S. Y. Park, and H. H. Lee, Adv. Mater. (Weinheim, Ger.) **14**, 1383 (2002).
[24] H. Schmid, H. Wolf, R. Allenspach, H. Riel, S. Karg, B. Michel, and E. Delamarche, Adv. Funct. Mater. **13**, 145 (2003).
[25] J. K. Diao, K. Gall, M. L. Dunn, and J. Zimmerman, Acta Mater. **54**, 643 (2006).
[26] J. K. Diao, K. Gall, and M. L. Dunn, Nano Lett. **4**, 1863 (2004).